Wind Energy

WILEY

RESEARCH ARTICLE OPEN ACCESS

The Impact of LIDAR-Assisted Pitch Control on Floating Offshore Wind Operational Expenditure

Andrew J. Russell[1] | Jade McMorland[2] | Maurizio Collu[2] | Alasdair S. McDonald[3] | Philipp R. Thies[4] | Aidan Keane[5] | Alexander R. Quayle[6] | David McMillan[7] | James Carroll[7] | Andrea Coraddu[8]

[1]Industrial Doctoral Centre for Offshore Renewable Energy, School of Engineering, King's Buildings, University of Edinburgh, Edinburgh, UK | [2]Department of Naval Architecture, Ocean and Marine Engineering, University of Strathclyde, Glasgow, UK | [3]School of Engineering, King's Buildings, University of Edinburgh, Edinburgh, UK | [4]Faculty of Environment, Science and Economy Engineering, University of Exeter, Penryn Campus, Penryn, UK | [5]Wood Renewables, Glasgow, UK | [6]Flotation Energy Ltd, Edinburgh, UK | [7]Electronic and Electrical Engineering Department, University of Strathclyde, Glasgow, UK | [8]Faculty of Mechanical, Maritime and Materials Engineering, Delft University of Technology, Delft, The Netherlands

Correspondence: Andrew J. Russell (A.J.Russell-1@sms.ed.ac.uk) | Jade McMorland (jade.mcmorland@strath.ac.uk)

Received: 23 November 2023 | **Revised:** 9 August 2024 | **Accepted:** 16 August 2024

Funding: This work was funded by UK Research and Innovation as part of the EPSRC and NERC Industrial CDT for Offshore Renewable Energy (IDCORE), Grant number EP/S023933/1. The authors would also like to acknowledge EPSRC for funding this work through the Wind and Marine Energy Systems Centre for Doctoral Training under grant number EP/S023801/.

Keywords: failure rates | floating offshore wind | LIDAR-assisted pitch control | O&M | operational expenditure | wind turbine control

ABSTRACT

Floating offshore wind (FOW) is a renewable energy source that is set to play an essential role in addressing climate change and the need for sustainable development. However, due to the increasing threat of climate emergency, more wind turbines are required to be deployed in deep water locations, further offshore. This presents heightened challenges for accessing the turbines and performing maintenance, leading to increased costs. Naturally, methods to reduce operational expenditure (OpEx) are highly desirable. One method that shows potential for reducing OpEx of FOW is LIDAR-assisted pitch control. This approach uses wind velocity measurements from a nacelle-mounted LIDAR to enable feedforward control of floating offshore wind turbines (FOWTs) and can result in reductions to the variations of structural loads. Results obtained from a previous study of combined feedforward collective and individual pitch control (FFCPC + FFIPC) are translated to OpEx reductions via reduced component failure rates for future FOW developments, namely, in locations awarded in the recent ScotWind leasing round. The results indicate that LIDAR-assisted pitch control may allow for an up to 5% reduction in OpEx, increasing to up to 11% with workability constraints included. The results varied across the three ScotWind sites considered, with sites furthest from shore reaping the greatest benefit from LIDAR-assisted control. This work highlights the potential savings and reduction in the overall levelised cost of energy for future offshore wind turbine projects deliverable through the implementation of LIDAR-assisted pitch control.

1 | Introduction

Renewable energy plays a vital role in addressing the serious challenges of climate change and the need for sustainable development. Wind energy, specifically offshore wind, is set to play an essential role in the deployment of clean energy sources globally. Offshore wind has seen significant success in recent years, with 9.4 GW installed worldwide as of 2022 [1]. However, due to the increasing threat of climate emergency, there is a heightened demand for further deployment of wind turbines. At present, bottom-fixed wind (BFW) turbines are limited to a depth of water of 60 m [2]. Wind Europe estimates that around 80% of Europe's available wind resource lies within waters exceeding this depth [3], and FOW provides a viable solution for wind deployment in deeper areas.

FOW technology benefits from the knowledge gained through the successful deployment of BFW, presenting a promising path towards commercially viable FOW projects. However, introducing floating systems brings new obstacles and limitations, primarily concerning the operational phase of the project. Key challenges for the technology include wave sensitivity, maintainability, anchor and mooring cost/complexity, and turbine motion, as identified by NREL [4]. With the increasing demand for FOW, deployment sites are being driven to greater offshore distances and depths, with associated harsher environmental conditions and heightened accessibility challenges.

Recently, there has been growing concern about the finance and profitability of future FOW projects. Challenges such as the risk of new technology, increased inflation rates globally, shortage of components/materials/vessels and lack of an established supply chain in remote deployment areas are set to put an additional financial strain on future FOW projects. Therefore, it is vital to reap cost-saving benefits where possible. O&M can account for up to 30% of the total cost of energy for BFW sites, making it a key area for cost reduction. Recent estimates for FOW cost of energy (CoE) indicate that OpEx for FOW projects could potentially exceed 40% due to challenges surrounding environmental conditions, turbine motion and major component replacements [5]. However, there are a number of methods to reduce this impact and to allow effective, efficient and economically feasible O&M campaigns for FOW.

The implementation of LIDAR-assisted pitch control is one method that shows promise for reducing OpEx of FOW sites. This method uses nacelle-mounted LIDAR to gather wind velocity measurements upstream of the turbine, to enable feedforward control of FOWTs. This allows FOWTs to actuate their pitch, torque or yaw control systems in advance of the wind's impact. The greatest benefits delivered by LIDAR-assisted control have been achieved when assisting with blade pitch control in above-rated wind speed conditions [6–9]. One of the key deliverables resulting from LIDAR-assisted pitch control is reductions in the variations of structural loads. This is significant because this gives rise to more consistent loads, which are predictable and uniform across the structure, resulting in reduced fatigue, failure rates and, consequently, lifetime extension, which can lead to reduced maintenance activities and OpEx. This paper aims to use the loading standard deviation reductions obtained from a previous study of LIDAR-assisted pitch control [9] to quantify how they translate to OpEx savings for FOW.

This paper is structured as follows. Section 2 provides a background overview of floating offshore wind and the O&M challenges specific to the technology. Section 2 also briefly overviews the advantages of LIDAR-assisted control within FOW. Section 3 provides a review of the LIDAR-assisted control strategy, implementation, and previous results. Section 4 introduces the O&M methodology for this analysis with details of the vessel fleet, support structure, and case study locations. Section 5 provides the OpEx results using a bottom-fixed wind farm as a baseline comparison. Finally, Section 6 presents conclusions from the results and offers recommendations for future work.

2 | Background

2.1 | Floating Wind Maintenance Overview

It is widely cited that O&M costs can account for up to 30% of the total cost of energy within offshore wind [10]. Yet recent studies have estimated that, for FOW technology, this figure could increase to almost 40% [5], highlighting the need for an effective O&M strategy. NREL identified wave sensitivity, maintainability, anchor cost/complexity, mooring cost/complexity and turbine motion as the key challenges posed by FOWT sites [11].

The deep depths of FOW sites pose challenges for conventional major component replacement vessels [2], which are limited to 60-m depth. This gives rise to the need for alternative methods such as floating-to-floating transfer, floating cranes, self-hoisting equipment and off-site solutions such as tow to shore. The limited availability of appropriate port and grid infrastructure hampers the wider adoption of FOW. Many European ports and harbours lack the necessary capacity to handle the installation and maintenance demands of such assets, particularly in terms of cranage, vessels and personnel, which is a growing concern due to the rapid pace of BFW and FOW site deployment.

As sites move into deeper waters, the average distance to shore is also expected to increase. The average distance to shore (mainland Scotland) of the proposed ScotWind projects exceeds 70 km, with this further increasing for the FOW sites, while the average distance to shore of the current operational offshore wind farms is 18.7 km [12]. The increase in distance to shore is expected to have a significant impact on the accessibility of the sites. Accessibility is determined based on both the weather conditions and the duration of suitable weather windows. Travel time to site and the required weather window increase with distance to shore. The weather window is the duration of access required to safely attend the site, complete the repair and then return to shore. As this duration increases, the access to the site decreases. Rowell et al. [13] compared the accessibility of future ScotWind sites against that of currently operating wind farms (e.g., Moray East). This work used significant wave height (H_s) as the limiting factor, which was kept consistent for both FOW and BFW sites. The results indicated that accessibility for FOW sites will be challenging, particularly for those using a crew transfer vessel (CTV)–based approach.

In addition to the existing access limits, the wave and tidal-induced motion of the turbine could potentially further limit turbine access. Turbine motion is frequently referenced in scholarly works as a major obstacle in FOW O&M procedures [14]. Recent studies have analysed the potential impact of turbine motion within a number of sea states [15–17]. Most of these studies have concentrated on ascertaining turbine motion under severe weather circumstances, aiming to establish the platform survivability and the impact of turbine motion on degradation and fatigue. Nevertheless, the exploration of turbine motion for maintenance-related oceanic conditions (e.g., situations where significant wave heights are below 4 m [18]) remains relatively constrained.

When modelling O&M processes, it is crucial to consider this additional motion in order to ensure the health and safety of

technicians. Assessing the workability of the turbine requires taking into account additional weather and environmental factors such as the peak wave period (T_p) and the direction of the waves [14]. The movement of the turbine is also expected to affect the degradation rate of components, especially within the drivetrain.

2.1.1 | Workability

The concept of workability has been explored within the literature by CoreWind [19] and Scheu et al. [20], identifying the workability index (WI) for several different floating platform designs. Workability is a measure of how safe it is for technicians to perform maintenance on the asset in a number of sea states, which are a combination of H_s, mean wind speed (U) and T_p. Currently, there is no definitive guidance to determine an acceptable WI for offshore wind operations. This introduces a trade-off between site accessibility and technician health and safety.

For one sea state condition, individual WIs from different motion directions (lateral, vertical and rotational) are calculated and multiplied to provide the WI of the specific H_s-T_p combination. The resulting WI is calculated for each H_s-T_p combination of interest. A WI of 1 indicates no impairment of working conditions due to motion, and a value of 0 means that work is not possible under the respective conditions. Time workable conditions are determined based on the specific response amplitude operator (RAO) of the selected offshore wind structure, under a specific set of H_s and T_p values. An acceptable motion threshold is then imposed based on the existing oil and gas threshold from Nordforsk [21]. This can then be normalised to allow for comparisons through the use of a workability index (WI):

$$WI = \frac{\sum T_{wc_i}}{T_t} \tag{1}$$

where T_{wc_i} is the number of workable hours and T_t is the total number of hours.

Scheu et al. [20] provided WI results for a 10-MW wind turbine mounted on four different platform designs (A, B, C, and D). Designs A–D include a spar, tension leg platform (TLP), semi-submersible and a barge design. However, the specific design details of A–D were not disclosed. Workability was found to be a slight limiting factor for sea states with a WI of $\leq 90\%$ and had a significant influence for WI < 60%. The concept of WI for specific platform designs was also explored within the CoreWind project [19]. This project examined the impact of two specific floater designs, ActiveFloat (semi-submersible) and WindCrete (spar). Both platforms were connected to a 15-MW–rated IEA reference turbine [22].

While existing guidance addresses safe human exposure, specific limits for a safe WI in offshore operations are lacking, though Scheu et al. [20] categorised WI impact >90% as slight, 60%–90% as significant and <60% as major.

In terms of operations, workability limits access to site, which in turn increases downtime due to an increase in "waiting on weather" periods. Floating sites are typically in areas with already challenging conditions, therefore the addition of more access limiting factors will have a negative impact on OpEx. One solution to overcome this challenge within the operational phase is to reduce the *number* of waiting on weather periods, by reducing the number of transfers taking place through failure rate reduction mechanisms.

2.2 | LIDAR-Assisted Control

One method that shows promise for reducing OpEx for FOW is LIDAR-assisted control. Nacelle-mounted, forward-facing LIDAR technology can provide measurements of the incoming wind field, the characteristics of which can be used for feedforward turbine control. Traditionally, turbines use feedback control. However, the drawback of this type of control strategy is that the wind turbine provides a delayed reaction to the incoming wind. Feedforward control is able to overcome this drawback by enabling turbines to actuate their control systems in advance of the wind's impact upon the rotor.

The greatest benefits delivered by LIDAR-assisted control have been observed when assisting with blade pitch control in above-rated conditions wind speed [6–8]. LIDAR-assisted feedforward pitch control has demonstrated an ability to enhance turbine performance through improved rotor speed regulation, and therefore more stable power capture. It is also capable of reducing the variation in the structural loadings, motions, and the tensions of the mooring lines of FOWTs [6–8, 23, 24].

Furthermore, wind turbines can utilise individual blade pitch control (IPC), which can mitigate the cyclic loads resulting from variations in the wind profile across the rotor-swept area caused by wind shear, wind veer and turbulence. The concept of feedback IPC (FBIPC) was first explored by Bossanyi et al [25] and applied to floating turbines by Namik and Stol [26]. Alternatively, feedforward individual pitch control (FFIPC) is able to deliver individual pitch commands in advance of the wind's impact and has been studied using various implementations [27–30]. In previous work, the benefits of LIDAR-assisted combined feedforward collective and individual pitch control (FFCPC + FFIPC) for a 15-MW floating offshore wind turbine were investigated [9]. Significant benefits to the turbine performance, loading and motion parameters were observed.

Building on the results of the previous work [9], this paper focuses on translating the reductions in the variations of the structural loads to component failure rate reductions and, subsequently, investigating how these can lead to reduced OpEx. The reductions in OpEx are expected to stem from the decreased lost revenue resulting from reduced downtime of turbines, as well as reduced costs associated with the reduced frequency of maintenance operations, where vessel hire, personnel and material costs are incurred. Furthermore, the reduced failure rates achieved from LIDAR-assisted control may also alleviate the workability access constraints for FOWTs due to the reduced frequency of transfers to site.

2.3 | ScotWind Case Study

In 2022, Crown Estate Scotland launched ScotWind Leasing, aiming to secure 8–10 GW of additional offshore wind capacity, raising the Scottish target to 17–19 GW, mainly by 2030–2032. The 2022 ScotWind leasing results exceeded expectations by awarding 11 floating projects with a combined capacity of approximately 18 GW [31], showcasing the rapid growth of the floating offshore wind industry and Scotland's leading position in this sector. The number of projects is expected to lead to significant competition when securing a strike price through contracts for difference (CfD). In addition, margins are tightened due to inflation and rising costs of commodities. Therefore, any technologies with potential OpEx reduction are of vital importance.

This work uses three of the recent ScotWind allocation sites as the basis of the case study: E1, NE1 and NE3. These sites have been selected due to their spread of location, capacity and distance to shore. This study aims to assess how the cost-saving benefits brought by LIDAR-assisted control differ for the three sites due to these variables. The location of these zones, with details of distance to shore and met-ocean averages, is provided in Table 1.

Further distances from shore require larger weather windows to allow for the longer travel time require to get to and from the site, which results in greater costs for vessel hire and personnel. Furthermore, the weather window restrictions for these far offshore locations amplifies the impacts of turbine downtime, as the waiting on weather periods will be longer and more frequent. Therefore, E1 is expected to benefit most from the implementation of the LIDAR-assisted control strategy because the reduced failure rates will not only decrease the downtime of the turbines, but also the frequency of maintenance visits and therefore the OpEx compared to using the feedback-only control strategy.

TABLE 1 | Case study ScotWind FOW regions with detail of O&M base, distance to shore and average H_s.

ScotWind site	O&M base	Distance to shore, km	Average H_s, m
E1	Aberdeen	120	1.7
NE1	Lerwick	55	1.5
NE3	Wick	55	1.6

3 | Operation and Maintenance Methodology

OpEx is defined as the cost of the operational phase of a project [32]. This is one of the few costs which can be controlled once the FOW farm is operational and is estimated to contribute up to almost 40% of the total cost of energy for future floating wind [5].

The OpEx simulations within this work were performed using the Strath-OW O&M model [33]. This model has previously been validated and used to assist in the development of maintenance campaigns for currently operational offshore wind farms [34]. This model has been adapted to account for workability limits imposed based on the platform design of FOWTs, as discussed in Section 2.1.

The model uses a Monte Carlo time domain simulation approach and consists of four input modules: climate, vessel specifications and fleet configuration, wind farm/turbine and cost and failures. For this analysis, the model has been adapted for FOW day-to-day maintenance procedures, excluding major replacement procedures.

This model comprises of three main parts: climate modelling, turbine failure modelling and resource and cost modelling. Users input sample data, allowing the model to simulate wind speed and significant wave height time series over the defined wind farm lifetime using a multivariate autoregressive model. These values play a crucial role in calculating energy production and losses, as well as determining turbine accessibility for maintenance tasks.

Within the current model [33], access to site is limited by U and H_s, where the thresholds are vessel dependent. Within this adapted model, where workability limits are imposed, the combination of T_p and H_s form the limiting criteria, dependent on the specific platform design. An example of limitations imposed for Design A [20] is shown in Figure 1.

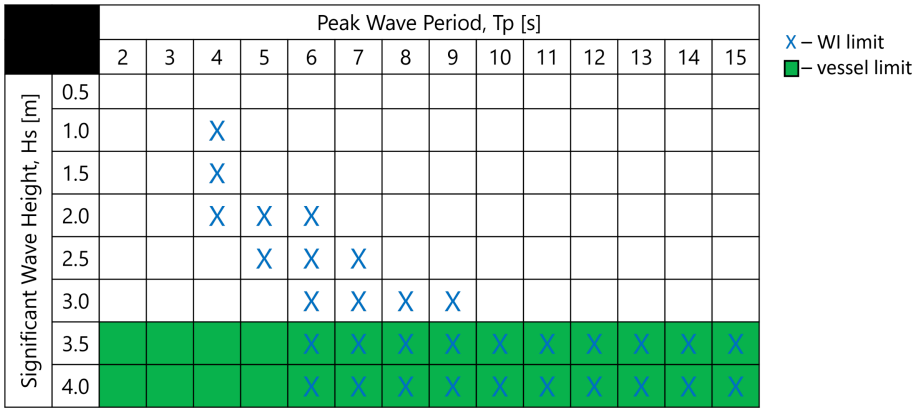

FIGURE 1 | Limitations imposed on accessibility for specific H_s-T_p combinations for Design A [20].

3.1 | Maintenance Strategy

Within offshore wind, maintenance actions can be categorised as minor, major or replacement operations [35, 36]. While there are significant challenges surrounding the major component replacement for FOW turbines, this work focused on the impact of reduced failure rates on minor/major repairs, which make up 90% of total failure rates [35]. Therefore, the use of a heavy lift vessel (HLV) was not included.

It was assumed that the cost of repair of components was identical for both BFW and FOW to allow for direct comparison. Each turbine had a 15-MW rating, based on the NREL 15-MW reference turbine [22]. All baseline failure rates, technicians required, time to repair and cost of components for different turbine subsystems were taken from Carroll et al. [35].

To allow for direct comparison between the ScotWind locations, each site had a capacity of 1 GW and followed the same maintenance strategy. Due to the scale of the sites, and distance to shore, the case study utilised a service operation vessel (SOV)–based maintenance strategy. Each site had a dedicated SOV, which was supported by daughter craft. A set of 6 daughter crafts was chosen to ensure that maintenance activities were not hindered due to resource limitations. The SOV and daughter craft had a H_s limit of 3.5 m and 2 m respectively. Since the goal of this study was to assess potential OpEx reductions via the implementation of LIDAR-assisted control, the optimisation of the vessel fleet was not the focus. Scheduled maintenance was set to 60 h per turbine per year. Maintenance activities were not limited by daylight working hours.

3.1.1 | OpEx Modelling

The adapted O&M model [33] is utilised within this analysis to determine potential OpEx savings of introducing LIDAR-assisted control, particularly within the context of floating wind. OpEx costs are commonly categorised into direct and indirect expenditures. Direct costs encompass fixed expenses, transportation fees, staffing outlays and repair costs. Conversely, indirect costs involve foregone earnings, termed as downtime, constituting a substantial portion of the overall OpEx. Downtime represents an opportunity cost, reflecting the revenue forgone due to asset failure, mirroring potential turbine-generated income [37].

Downtime is dependent on two factors, frequency of failure and accessibility. As the number of failures increase, the number of periods of downtime increase, therefore leading to an increase in lost revenue. However, the duration of downtime can be increased due to poor access to site. Due to safety limitations imposed on operation, turbines can only be repaired in periods of favourable weather.

This is particularly challenging for floating turbines, due to additional workability limitations imposed due to the floating platform but also due to their greater distances from shore making access more restricted by weather windows as personnel have to be offshore for longer periods of time compared to BFW. A reduction in failure rates will have a benefit for both BFW and FOW sites, due to reductions in downtime, in addition to repair costs, transfer costs and fuel costs. However, the most significant benefit is expected for sites with poor accessibility, which will be more common for FOW, where the cost of a single maintenance action is high due to waiting on weather periods. The failure rate reductions brought by LIDAR-assisted control can help to reduce OpEx costs by reducing the frequency of trips required to perform repairs, thereby leading to savings in vessel hire, personnel, fuel and repair costs.

4 | LIDAR-Assisted Control Methodology

The turbine studied within aero-servo-hydro-elastic simulations was the IEA-Wind 15-MW reference turbine, developed between NREL and the Technical University of Denmark (DTU), via the IEA, as defined by Gaertner et al. [22]. The turbine was mounted on the University of Maine's VolturnUS-S semi-submersible [38]. The FOWT was simulated using NREL's open-source Fatigue, Aerodynamics, Structures, and Turbulence (FAST) code. OpenFAST is the latest iteration of the FAST code, and version 3.4 was used for this study, with modifications made to allow for LIDAR configuration simulation within the InflowWind module, which are now present within OpenFAST, from version 3.5 onwards. The LIDAR measurements were interfaced to ServoDyn and sent to the Reference Open Source Controller (ROSCO) [39] where v2.6 was modified to enable LIDAR-assisted control. Full descriptions of the modifications made to OpenFAST and ROSCO were disclosed in previous work [9]. Due to its large rotor diameter (240 m), the turbine is subject to significant variations in structural loads due to differences in the wind profile across the rotor-swept area. In order to mitigate these variations, individual feedforward pitch control was also implemented within the ROSCO controller and worked by providing additional tuning to the pitch of each blade depending on its azimuth position. Full explanation of the feedforward collective and individual pitch control theory can be found within the previous work [9]. The combined feedforward collective and individual pitch controller (FFCPC + FFIPC) was found to deliver significant benefits to the performance, motions and loadings of the FOWT, by way of standard deviation (σ) reductions, compared to the baseline feedback-only (FB) controller, the collective pitch controller (FFCPC) and the FFCPC combined with a traditional feedback individual pitch controller (FFCPC + FBIPC) across the full above-rated wind spectrum, as shown in Figure 2.

From Figure 2, the addition of FFCPC + FFIPC was able to deliver significant benefits to turbine and substructure parameters across the above-rated wind spectrum. Key reductions were observed in the rotor speed and power, as seen in Figure 2a, due to the superior blade pitch preparation in advance of the wind impact. This resulted in up to 56% reductions in their standard deviations compared to the baseline. The superior turbine performance had positive benefits on the bending moments acting on the turbine (Figure 2b), with reductions in the standard deviations of over 15% recorded in the rotor total load and the tower base fore-aft bending moment compared to the baseline controller. The benefits to the

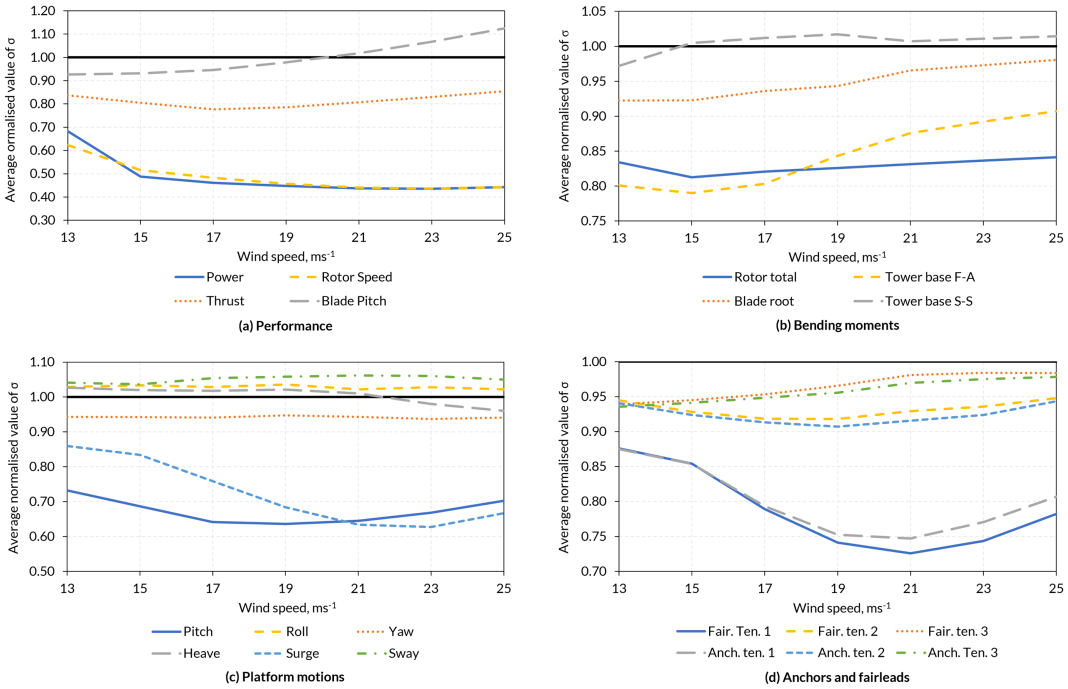

FIGURE 2 | Normalised values of σ for various turbine and substructure parameters when using FFCPC + FFIPC compared to the baseline feedback controller (denoted by black lines at 1.00). Values shown are averaged values from four random seed 1-h simulations at each average wind speed integer.

loadings were particularly relevant to this work, as the standard deviation reductions can lead to reduced failure rates and damage equivalent loads (DELs) of the turbine's components. Moreover, positive benefits were also observed in the platform motions (Figure 2c), namely, in pitch and surge, due to the reductions in the variation in the thrust force acting on the turbine. These benefits also translated to the mooring line tensions at the anchors and fairleads (Figure 2d).

4.1 | Failure Rate Determination

The results of the feedback-only controller and the best-performing feedforward controller examined in the previous work (FFCPC + FFIPC) were post-processed using MLife. MLife is a MatLab-based tool created by NREL to post-process results from wind turbine tests and aero-elastic, dynamic simulations, including from OpenFAST. MLife computes statistical information and fatigue estimates for one or more data files and follows the techniques outlined in the industrial standards [40]. Essential details and equations detailing MLife's operation are provided here. A complete theory manual by Hayman [41] outlining all details of MLife's operation is also available for reference.

MLife works by accumulating fatigue damage due to fluctuating loads over the design life of a wind turbine, which are broken down into individual hysteresis cycles by rainflow counting [41]. The damage is assumed to accumulate linearly with each cycle according to Miner's rule. The total damage from all cycles is given by

$$D = \sum_i \frac{n_i}{N_i\left(L_i^{RF}\right)} \tag{2}$$

where N_i is the number of cycles to failure, n_i is the cycle count and L_i^{RF} is the cycle's load range about a fixed load-mean value. The relationship between the load range and cycles to failure (the S-N curve) is modelled by

$$N_i = \left(\frac{L^{ult} - |L^{MF}|}{\frac{1}{2}\left(L_i^{RF}\right)}\right)^m \tag{3}$$

where L^{ult} is the ultimate design load of a component, L^{MF} is the fixed load-mean and m is the Wöhler exponent, which is specific to the component under consideration. In this study“ an m of 4 was used for steel components and an m of 10 was used for composite components.

As the simulations performed only cover a short period of the design lifetime, the time-series damage-cycle counts must be extrapolated over the design lifetime. To perform these extrapolations of the damage-cycle counts across the lifetime of the wind turbine, MLife requires the wind speed distributions of the sites. This enables MLife to model the wind with a Weibull distribution. The Weibull parameters and average wind speeds inputted to MLife for each of the ScotWind sites analysed are given in Table 2.

The wind speeds were then placed into bins, which were then assigned a probability of occurrence based on the Weibull distribution for each site. Following the lifetime extrapolation, the total damage was determined [41]. As failure occurs when D^{Life} equals one, the time until failure, T^{Fail}, is the ratio between the design lifetime and the accumulated damage.

$$T^{Fail} = \frac{T^{Life}}{D^{Life}} \tag{4}$$

TABLE 2 | Average wind speeds and Weibull parameters of the ScotWind leasing locations assessed in this study [42].

ScotWind site	Average wind speed, $m\,s^{-1}$	Weibull scale parameter C	Weibull shape parameter K
E1	8.293	9.358	2.360
NE1	8.567	9.667	2.394
NE3	10.10	11.39	2.255

TABLE 3 | Turbine subsystems considered in this study and the OpenFAST outputs associated with them.

Sub-system	OpenFAST output	Description	Units
RNA[a]	RtFldMxh	Total rotor aerodynamic load (moment in x direction)	Nm
Pitch bearings	RootMxc#	Blade in-plane moment at the blade root[b]	kN m
	RootMyc#	Blade out-of-plane moment at the blade root[b]	kN m
Blade roots	RootMxb#	Blade edgewise moment at the blade root[b]	kN m
	RootMyb#	Blade flapwise moment at the blade root[b]	kN m
Tower base	TwrBsMxt	Tower base side-to-side bending moment	kN m
	TwrBsMyt	Tower base fore-aft bending moment	kN m
Moorings	FAIRTEN1	Tension in mooring line 1 at the fairlead	kN
	ANCHTEN1	Tension in mooring line 1 at the anchor	kN

[a]RNA is assumed to represent the rotor blades, hub and pitch system.
[b]# is the blade number from 1 to 3.

The failure rate, λ, is the inverse of the time until failure.

$$\lambda = \frac{1}{T^{Fail}} \tag{5}$$

Within the analysis performed in this study, the time series outputs for numerous loadings associated with different turbine components were inputted to MLife and the time to failure associated with each loading on a component was determined. The loading with the lowest time to failure was assumed to be the time to failure for the component.

4.2 | Assessed Parameters

OpenFAST allows for the output of time-series data of numerous loadings applied to the turbine's various subsystems. These include the rotor blades, tower, shaft, bedplate and pitch bearings. The data acquired can be processed through MLife, which can return the damage, time to failure and DEL occurring as a result of a particular load applied on the subsystem. As the OpenFAST load outputs are defined at various cross sections of the turbine, this process works well for structures composed of simple cylindrical shapes and isotropic materials such as the tower and shaft, as S-N curves are able to deliver a good indication of the time to failure at the cross sections of the components. Conversely, for non-cylindrical components, MLife is unable to accurately predict their times to failure as the S-N curves cannot be applied to these components. A detailed finite element analysis, with the load outputs from OpenFAST as an input, is required to determine the resulting state of stress for these components. However, for the purposes of this study, the total aerodynamic load-induced bending moments on the rotor-nacelle assembly (RNA) was assumed to represent the forces acting upon the rotor blades, hub and pitch system, as defined by Dao et al. [43]. The approximately 15% reductions to the standard deviation of these loads (Figure 2) were, therefore, used to estimate the reductions to the times to failure of the components within the RNA, which will be used within the O&M model.

Table 3 gives the OpenFAST outputs that represent the loadings applied to the relevant sub-system. Time-series data of these outputs obtained from average turbulent wind speeds of 11–25 $m\,s^{-1}$ in intervals of 2 $m\,s^{-1}$ were inputted to MLife for the turbine utilising the FB or FFCPC + FFIPC controllers. For the FFCPC + FFIPC, the same data as was used for the FB when average wind speeds below 11 $m\,s^{-1}$ were simulated as this was below the rated wind speed (10.69 $m\,s^{-1}$) and where the feedforward controller did not operate.

At each average wind speed integer from 3 to 25 $m\,s^{-1}$, four random seed 1-h simulations were performed. The turbulence was generated under the normal turbulence model (NTM), turbulence intensity (TI) category B using TurbSim [44]. These conditions fall into design load case (DLC) 1.2, as defined in the industrial standards [40]. DLC 1.2 was used as this embodies the loads resulting from turbulence that occurs during the normal operation of a wind turbine throughout its lifetime. The floating turbine was modelled in a water depth of 200 m and under irregular waves. The wind and waves were aligned

in the same direction. Though normally a joint probability distribution of wind and waves is considered within DLC 1.2 for lifetime fatigue estimates, this was not performed within this study because the OpEx reduction results presented in Section 5 focus solely on the loading reductions experienced by the rotor, which is assumed to be aligned with the wind direction at all times. However, a joint wind and wave probability distribution should be considered when further investigating the benefits to the tower and moorings. H_s and T_p were adjusted to suit each average wind speed integer, with values interpolated from those defined by Allen et al [38], and shown in Table 4.

When analysing the time-to-failure data for the subsystems with multiple relevant loading outputs outlined in Table 3, namely, the pitch bearings, the blade roots and the tower base, a first-to-fail approach was taken such that the loading with the lowest time-to-failure was used for comparison between the FB and FFCPC + FFIPC control strategies.

5 | Results and Discussion

Within this section, the reduction of failure rates through LIDAR implementation is discussed. The impact of these reductions is then quantified through simulation of OpEx over a lifetime of a given site.

5.1 | LIDAR-Assisted Control Failure Rate Reductions

The results of the MLife post-processing using the data from the four random seed 1-h simulations are shown in Table 5. Results are presented as normalised values of failure rate compared to the baseline feedback-only controller.

The loadings resulting in the lowest time-to-failure of subsystems in Table 5 occurred in the fore-aft direction due to the alignment of the FOWT with the co-directional wind and waves. Table 5 indicates that the FFCPC + FFIPC strategy was able to deliver significant reductions to the failure rates of turbine subsystems at all of the investigated sites. The reductions in the failure rate of the tower base may not be significant for O&M costs due to their relatively low failure rate, but indicate potential for structure optimisation, whereby a thinner, lighter tower may be possible. The results also highlighted the promising potential to enable failure rate reductions of the pitch bearing, the blade roots and the mooring system. While it was found within the previous work that the standard deviation of the blade pitch increased at higher above-rated wind speeds [9], as shown in Figure 2, this is believed to have been offset by the reduced standard deviations of the blade pitch at lower above-rated wind speeds, which represent a much greater proportion of the probability distribution of wind speeds than at higher wind speeds, ultimately resulting in the reduced failure rates of the pitch bearing. However, it is worth noting that the failure rate reduction reported here is solely based on the loadings imparted on the components and so does not account for failures arising from mechanical wear of the pitch system from control actuation.

For the purpose of this study, the most significant result was that of the rotor total load leading to failures in the RNA. For each of the sites, an approximately 20% reduction in the failure rate resulting from the rotor total load was recorded. The results also indicated marginally greater reductions in the failure rate at site NE3 than at sites NE1 and E1. This was due to its slightly higher average wind speed at the site (as shown in Table 2), meaning

TABLE 4 | IEC DLC 1.2 NTM wind and wave conditions [38].

U_{hub}, m s^{-1}	3	5	7	9	11	13	15	17	19	21	23	25
H_s, m	1.10	1.14	1.25	1.43	1.69	2.01	2.39	2.83	3.34	3.82	4.27	4.80
T_p, s	8.52	8.41	8.16	7.83	7.55	7.45	7.55	7.85	8.28	8.75	9.22	9.70

TABLE 5 | Normalised values of failure rates for turbine subsystems resulting from the loads recorded by the OpenFAST simulation outputs when using FFCPC + FFIPC relative to the baseline FB controller at each ScotWind site.

		Normalised failure rate			
Subsystem	**OpenFAST output**	**Baseline**	**E1**	**NE1**	**NE3**
RNA[a]	RtFldMxh	1.00	0.81	0.80	0.79
Pitch bearings	RootMyc#[b]	1.00	0.56	0.55	0.54
Blade roots	RootMyb#[b]	1.00	0.57	0.57	0.57
Tower base	TwrBsMyt	1.00	0.73	0.72	0.70
Moorings	FAIRTEN1	1.00	0.92	0.91	0.90
	ANCHTEN1	1.00	0.92	0.91	0.90

Note: Outputs correspond to the loadings with the lowest time-to-failure for each subsystem when using the baseline FB controller, hence the omission of the other outputs present in Table 3.
[a]RNA is assumed to represent the rotor blades, hub and pitch system.
[b]# is the blade number from 1 to 3. Values are averages.

that more of its lifetime will be spent with the feedforward controller operating in above-rated wind speeds where the loading reductions can be achieved.

5.2 | Baseline Comparison

As discussed in Section 5.1, the LIDAR simulations saw a reduction in degradation and failure rates for the RNA, pitch bearings, blade roots, tower base and mooring system. Within the literature surrounding offshore wind turbine failure rates, there is a variety of nomenclature used, making it difficult to draw comparison between the results. In the review by Dao et al. [43] the definition of RNA is made up of the subassemblies of blades, hub, air brake and pitch system. These elements were matched to the failure rates for the subassemblies detailed in the work of Carroll et al. [35]. For all FOW simulations, the failure rates for the RNA only are adjusted based on the normalised values presented in Table 5. The same failure rate reductions were assumed to apply to all wind turbines within the array. All other failure rates are that of the BFW equivalent site [35].

OpEx encompasses all expenses incurred from the moment of takeover, comprising both one-time and recurring costs associated with the wind farm, measured annually. These costs are split as direct and indirect costs. Direct costs are those which have a "direct" impact on the operation of the site finances such as cost of repair, transport, staff and other fixed costs such as insurance. Indirect costs, such as lost production costs are more difficult to predict, due to uncertainty in the prediction of unscheduled failures and metocean conditions. Lost revenue is viewed within industry as an "opportunity cost". An opportunity cost is defined as the revenue which could have been generated, had the turbine been operational.

The reduction in total OpEx, and the subcosts for a FOW farm with the reduced failure rates obtained from the implementation of LIDAR-assisted control are given in Table 6. This analysis is based on vessel limits only using the existing Strathclyde O&M model [33].

The study's outcomes indicate a notable 3%–5% reduction in operational expenditures, displaying variability among different sites. Particularly, NE3 emerges as the most advantageous because this exhibiting the most substantial decrease in RNA failure rates compared to the other locations (Table 5) due to its higher average wind speeds, meaning that LIDAR-assisted control is active for a greater proportion of its lifetime. The overall decline in OpEx is attributed to lowered lost revenue, due to reduced downtime, and repair expenses. The key OpEx costs savings result from the potential for transport costs to be reduced by decreasing the number of vessels (and associated hiring costs) due to the reduced required transfers resulting from the lifetime extension of the components. The relationship between the reduction of failure rates, and therefore number of transfers required, and the OpEx decrease is highlighted in Figure 3. This illustrates that as the reduction to the failure rate achieved from LIDAR-assisted pitch control increases, the OpEx savings increase because fewer transfers to the wind farm site are required during the lifetime, thereby reducing costs of vessel hire and personnel. The reduced failure rates also mean that components require repair less frequently, resulting in the repair cost savings shown in Table 6.

TABLE 6 | OpEx savings breakdown based on reduction of failure rates.

	E1	NE1	NE3
Lost revenue	5.38%	8.58%	1.70%
Repair costs	7.10%	10.3%	11.0%
Total OpEx	2.89%	4.29%	5.05%

These results are representative of the impact of the reduced failure rates on the WindCrete and ActiveFloat [19] designs, where workability would not impact operation using an SOV strategy with a H_s limit of 3 m.

5.3 | Workability Impact

As previously discussed in Section 2.1.1, FOW turbines are also subject to additional weather constraints due to human exposure to the motion of the asset. As shown in Figure 1, workability limitations are unique to each platform design and limits access to the turbine during specific combinations of T_p and H_s. Using designs A-D from Scheu et al. [20], the workability limitations are imposed on access to the site, in addition to the existing vessel limits. As previously discussed, CoreWind [19] also provides WI limitations for the ActiveFloat semi-sub and WindCrete spar designs. However, these limitations only exist for WI combinations of 3.5 m and above, which are already captured within the vessel limits; therefore, the OpEx results will be unchanged from those presented in Table 6. The methodology detailing the adaptations can be found in previous work [45].

Within this analysis, the WI limitations are placed on both the FOW baseline comparison and the FOW with reduced failure rates due to the LIDAR-assisted control implementation. It is assumed that any H_s-T_p combinations resulting in WIs less than 1 are inaccessible. The estimated OpEx savings are shown in Figure 4.

Unlike the results with no consideration of WI, the highest OpEx savings is not consistent with the site with the highest

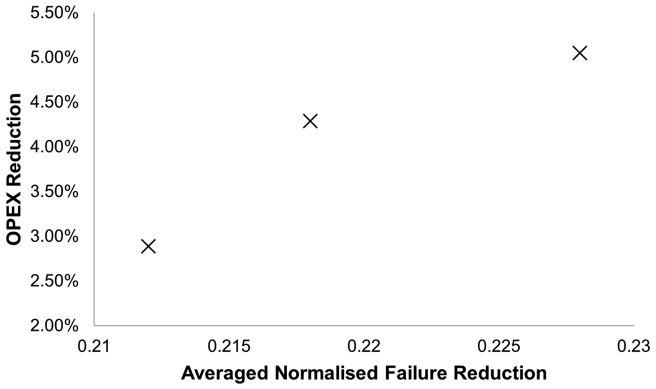

FIGURE 3 | Relationship between failure rate reduction of the RNA and OpEx savings.

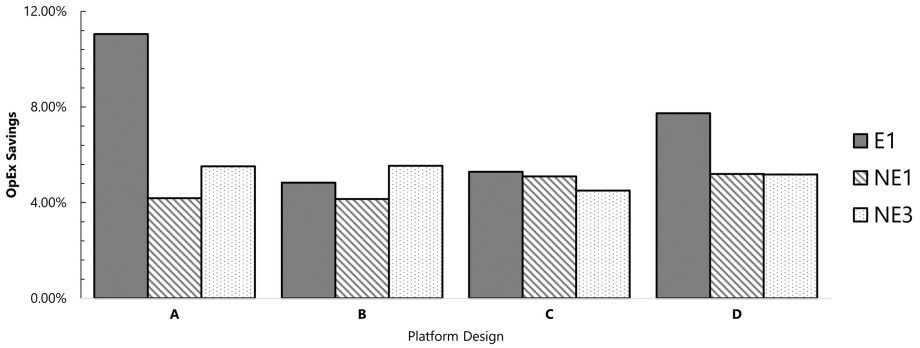

FIGURE 4 | OpEx savings resulting from reduced failure rates for FOW sites with imposed WI limitations.

TABLE 7 | Percentage savings in OpEx from FOW with WI limits and LIDAR-assisted control enabled failure rate reductions compared to the equivalent BFW baseline using feedback-only control, where "—" indicates that the BFW was cheaper than the FOW equivalent site.

ScotWind site	Design A	Design B	Design C	Design D
NE1	—	—	1.89%	—
NE3	4.41%	4.97%	4.57%	0.39%

Note: FOW was not more cost-effective at E1 for any of the designs.

reduction in failure rates. Site E1 has the highest OpEx savings for all platform designs.

Site E1 experiences the highest OpEx primarily because it undergoes the most significant reduction in accessibility resulting from the incorporation of workability limits. As a result, it reaps the most substantial advantage from the decrease in failure rates. This advantage translates into a reduction in the necessary transfers and subsequently minimises the demand for optimal weather conditions. This highlights that sites with accessibility challenges, and therefore predicted high OpEx, can see the highest benefit from the addition of LIDAR-assisted control.

The variability of the results for the 4 designs highlights the unique challenges of each specific design, and that there is no "one-fits-all solution." As with the comparison in Table 6, for LIDAR-assisted control with no WI considerations, the decrease in OpEx is attributed to the reduction of repair costs and lost revenue. However, for all sites and all designs, the savings in lost revenue was the main contributor to these savings, due to the challenges of accessibility and the link between access and OpEx [46].

When comparing the FOW with both LIDAR-assisted control and motion limitations against the BFW equivalent with feedback-only control (i.e. without LIDAR-assisted control) for specific designs, in some cases, the total OpEx for motion limited FOW with LIDAR-assisted control delivered failure reductions was less than that of the BFW with original failure rates and no motion limits. The percentage savings in OpEx for NE1 and NE3 are detailed in Table 7.

Site NE3 saw consistent savings across all designs, whereas NE1 was only more cost-effective than BFW equivalent for Design C. E1 was not found to be more cost-effective for any of the designs due to the additional workability restrictions of the FOW site, which resulted in larger costs than the BFW equivalent despite including the failure rate reductions brought by the LIDAR-assisted control.

The results show that while FOW the sites face additional challenges due to location and motion, the implementation of specific technologies and control strategies, such as LIDAR-assisted control, has the potential to bring certain aspects of the cost of some FOW sites below that of the equivalent BFW site using feedback-only control.

6 | Conclusions

This work has highlighted the potential OpEx benefits from the introduction of a LIDAR control strategy for future FOW developments. While implementing a LIDAR system incurs initial capital costs, its potential for substantial OpEx savings presents can justify the initial expenditure. In addition to the OpEx saving, there is the additional benefit of the reduction in the number of transfers within a health and safety context. Reducing the number of transfers, in turn, will reduce the total exposure to motion for technicians on FOW turbines, and therefore have a well-being impact. The reduction in transfers also allows for the vessel fleet to be optimised and potentially reduced, resulting in savings in transportation costs and in vessel emissions.

The key findings from this work can be summarised as follows:

- The LIDAR-assisted pitch control simulations performed within OpenFAST indicated the ability to deliver reductions in the failure rate of components in the rotor nacelle assembly by 20%, the tower base by up to 30% and the pitch bearings and blade roots by 46%. These translated to baseline OpEx savings of up to 5%.

- FOW sites most impacted by the addition of WI limits saw the largest OpEx savings from LIDAR-assisted control integration due to the reduction in downtime and lost revenue.
- For specific designs and sites, the overall OpEx for FOW sites with motion limits and LIDAR-assisted control were more cost-effective than the BFW equivalent site using feedback-only control.

Within this work, the focus has been surrounding the OpEx savings of the reduction of failures for the RNA for minor and major repairs using an SOV vessel supported by a fleet of daughter craft. However, as highlighted, the moorings, blade root, pitch bearing and tower also experience a reduction in fatigue due to the implementation of LIDAR-assisted pitch control, and therefore, the potential OpEx savings highlighted here could be increased.

While minor/major repairs can account for up to 90% of the total failure rates, the cost associated with major component replacements makes up a significant portion of the total OpEx for the full site lifecycle. It is expected that major component replacement for FOW has the potential to be highly costly due to the time involved in a tow to shore operation, or the cost of specialist vessels for in situ maintenance. Therefore, the reduction in failures for these maintenance events could have significant operational savings.

To summarise, the integration of LIDAR-assisted control in floating wind turbine projects emerges as a promising solution to mitigate failure rates and subsequently drive down OpEx. By accurately assessing environmental conditions and adjusting turbine operations in real-time, LIDAR technology offers a proactive approach to enhancing overall system reliability. The quantification of OpEx reduction resulting from decreased failure rates highlights the potential savings, and reduction in the overall levelised cost of energy for future FOW developments.

The results presented assume 100% LIDAR availability and therefore should be considered to be the best case scenario for the benefits delivered by this LIDAR-assisted control approach. Further work should seek to perform sensitivity analysis to investigate the impact of reduced LIDAR availability and LIDAR-assisted pitch control benefit on the failure rates and cost savings. Further work may also seek to address the potential for structural optimisation of the turbine and substructure through the implementation of LIDAR-assisted control, as well as how nacelle-mounted LIDAR wind measurement can help in understanding the loadings on FOWTs in their inactive (feathered blades) state.

Author Contributions

Andrew Russell performed the modifications to the OpenFAST and ROSCO source codes, executed the OpenFAST simulations, MLife post-processing and compiled the LIDAR-assisted control related aspects of the paper. **Jade McMorland** performed the O&M modelling and compiled the O&M related aspects of the paper. **Maurizio Collu, Alasdair McDonald, Philipp Thies, Aidan Keane, Alexander Quayle, David McMillan, James Carroll** and **Andrea Corradu** provided supervision, suggestions and reviewed the paper.

Acknowledgements

This work was funded by UK Research and Innovation as part of the EPSRC and NERC Industrial CDT for Offshore Renewable Energy (IDCORE), Grant number EP/S023933/1. The authors would also like to acknowledge EPSRC for funding this work through the Wind and Marine Energy Systems Centre for Doctoral Training under grant number EP/S023801/.

Conflicts of Interest

The authors declare no conflicts of interest.

Data Availability Statement

The original modified version of OpenFAST v.3.4, which includes the LIDAR simulator used in this work can be accessed via https://github.com/Russell9798/OpenFAST-v3.4-Lidar-IfW-Original/releases/tag/2.0. The modified version of ROSCO v2.6 with the feedforward control additions can be accessed via https://github.com/Russell9798/ROSCO-v2.6-LAC-IPC/releases/tag/2.0.

LIDAR-assisted control simulation datasets used for this paper are available and can be assessed via https://doi.org/10.17605/OSF.IO/FE6YP.

Peer Review

The peer review history for this article is available at https://www.webofscience.com/api/gateway/wos/peer-review/10.1002/we.2951.

References

1. World Forum Offshore Wind, "Global Offshore Wind Report," (2022), https://wfo-global.org/wp-content/uploads/2023/03/WFO_Global-Offshore-Wind-Report-2022.pdf.

2. D. Ahn, S. Shin, S. Kim, H. Kharoufi, and H. Kim, "Comparative Evaluation of Different Offshore Wind Turbine Installation Vessels for Korean West-South Wind Farm," *International Journal of Naval Architecture and Ocean Engineering* 9, no. 1 (2017): 45–54.

3. Wind Europe, "Floating Wind Vision Statement," https://windeurope.org/wp-content/uploads/files/about-wind/reports/Floating-offshore-statement.pdf.

4. S. Butterfield, W. Musial, J. Jonkman, and P. Sclavounos, "Engineering Challenges for Floating Offshore Wind Turbines," tech. rep. National Renewable Energy Lab.(NREL), Golden, CO (United States, 2007).

5. BVG, "Guide to a Floating Offshore Wind Farm," https://guidetofloatingoffshorewind.com/wind-farm-costs/.

6. D. Schlipf, E. Simley, F. Lemmer, L. Pao, and P. W. Cheng, "Collective Pitch Feedforward Control of Floating Wind Turbines Using LIDAR," in *25th ISOPE International Ocean and Polar Engineering Conference* (2015), ISOPE–I–15–755.

7. S. T. Navalkar, J. van Wingerden, P. A. Fleming, and G. Van Kuik, "Integrating Robust LIDAR-Based Feedforward With Feedback Control to Enhance Speed Regulation of Floating Wind Turbines," in *2015 American Control Conference (ACC)* (IEEE, 2015), 3070–3075.

8. D. Schlipf, F. Lemmer, and S. Raach, "Multi-Variable Feedforward Control for Floating Wind Turbines Using LIDAR," in *30th ISOPE International Ocean and Polar Engineering Conference* (2020), ISOPE–I–20–1174.

9. A. J. Russell, M. Collu, A. S. McDonald, P. R. Thies, A. Keane, and A. R. Quayle, "Lidar-Assisted Feedforward Individual Pitch Control of a 15 MW Floating Offshore Wind Turbine," *Wind Energy* 27, no. 4 (2024): 341–362.

10. Y. Feng, P. J. Tavner, and H. Long, "Early Experiences With UK Round 1 Offshore Wind Farms," *Proceedings of the Institution of Civil Engineers-energy* 163, no. 4 (2010): 167–181.

11. W. Musial, S. Butterfield, and A. Boone, "Feasibility of Floating Platform Systems for Wind Turbines," in *42nd AIAA Aerospace Sciences Meeting and Exhibit*, (2004): 1007.

12. H. Díaz and C. G. Soares, "Review of the Current Status, Technology and Future Trends of Offshore Wind Farms," *Ocean Engineering* 209 (2020): 107381.

13. D. Rowell, B. Jenkins, J. Carroll, and D. McMillan, "How Does the Accessibility of Floating Wind Farm Sites Compare to Existing Fixed Bottom Sites?," *Energies* 15, no. 23 (2022): 8946.

14. B. Jenkins, A. Prothero, M. Collu, J. Carroll, D. McMillan, and A. McDonald, "Limiting Wave Conditions for the Safe Maintenance of Floating Wind Turbines," in *Journal of Physics: Conference Series*, Vol. 2018, (IOP Publishing, 2021): 12023.

15. C. M. Wang, T. Utsunomiya, S. C. Wee, and Y. S. Choo, "Research on Floating Wind Turbines: A Literature Survey," *IES Journal Part A: Civil & Structural Engineering* 3, no. 4 (2010): 267–277.

16. S. Bashetty and S. Ozcelik, "Review on Dynamics of Offshore Floating Wind Turbine Platforms," *Energies* 14, no. 19 (2021): 6026.

17. A. Otter, J. Murphy, V. Pakrashi, A. Robertson, and C. Desmond, "A Review of Modelling Techniques for Floating Offshore Wind Turbines," *Wind Energy* 25, no. 5 (2022): 831–857.

18. I. B. Sperstad, M. Stålhane, I. Dinwoodie, O.-E. V. Endrerud, R. Martin, and E. Warner, "Testing the Robustness of Optimal Access Vessel Fleet Selection for Operation and Maintenance of Offshore Wind Farms," *Ocean Engineering* 145 (2017): 334–343.

19. CoreWind, "Floating Wind O&M Strategies Assessment," (2020), https://corewind.eu/wp-content/uploads/files/publications/COREWIND-D4.2-Floating-Wind-O-and-M-Strategies-Assessment.pdf.

20. M. N. Scheu, D. Kaufer, M.-A. Schwarzkopf, and A. Kolios, "Workability on Offshore Wind Turbines—A Comparative Study of Fixed-Bottom and Floating Applications," in *ISOPE International Ocean and Polar Engineering Conference* (ISOPE, 2018), ISOPE–I.

21. I. R. Nielsen, "Assessment of Ship Performance in a Seaway," (1987). Publisher: NORDFORSK, Sortedam Dossering 19, DK-200 Copenhage, Denmark, ISBN: 87-982637-1-4.

22. E. Gaertner, J. Rinker, L. Sethuraman, et al., "Definition of the IEA-Wind 15-Megawatt Offshore Reference Wind Turbine," Tech. Rep. NREL/TP-5000-75698. (NREL, Golden, CO, 2020).

23. D. Schlipf, F. Guo, S. Raach, and F. Lemmer, "A Tutorial on LIDAR-Assisted Control for Floating Offshore Wind Turbines," in *2023 American Control Conference (ACC)*, (2023): 2536–2541.

24. F. Guo and D. Schlipf, "Assessing LIDAR-Assisted Feedforward and Multivariable Feedback Controls for Large Floating Wind Turbines," *Wind Energy Science Discussions* 2023 (2023): 1–25.

25. E. A. Bossanyi, "Individual Blade Pitch Control for Load Reduction," *Wind Energy* 6, no. 2 (2003): 119–128.

26. H. Namik and K. Stol, "Individual Blade Pitch Control of Floating Offshore Wind Turbines," *Wind Energy* 13, no. 1 (2010): 74–85.

27. D. Schlipf, S. Schuler, P. Grau, F. Allgöwer, and M. Kühn, *Look-Ahead Cyclic Pitch Control Using LIDAR* (University of Stuttgart, 2010).

28. S. Raach, D. Schlipf, D. Sandner, and P. W. Cheng, "Nonlinear Model Predictive Control of Floating Wind Turbines With Individual Pitch Control," in *2014 American control conference (ACC)*, (2014): 4434–4439.

29. F. Dunne, L. Pao, A. Wright, B. Jonkman, and N. Kelley, "Combining Standard Feedback Controllers With Feedforward Blade Pitch Control for Load Mtigation in Wind Turbines," in *48th AIAA Aerospace Sciences Meeting Including the New Horizons Forum and Aerospace Exposition*, (2010): 250.

30. F. Dunne, D. Schlipf, L. Pao, et al., "Comparison of Two Independent LIDAR-Based Pitch Control Designs," in *50th AIAA Aerospace Sciences Meeting Including the New Horizons Forum and Aerospace Exposition*, (2012): 1151.

31. Crown Estate Scotland, "Awards: Lead Applicants, Project Partners, Area, Capacity and Foundations," (2022), https://www.crownestatescotland.com/resources/documents/scotwind-list-of-successful-project-partners.

32. A. Ioannou, A. Angus, and F. Brennan, "Parametric Capex, Opex, and Lcoe Expressions for Offshore Wind Farms Based on Global Deployment Parameters," *Energy Sources, Part B: Economics, Planning, and Policy* 13, no. 5 (2018): 281–290.

33. I. Dinwoodie, F. Quail, and D. McMillan, "Analysis of Offshore Wind Turbine Operation and Maintenance Using a Novel Time Domain Meteo-Ocean Modeling Approach," *Turbo Expo: Power for Land, Sea, and Air*, Vol. 44724 (American Society of Mechanical Engineers, 2012), 847–857.

34. I. Dinwoodie, O.-E. V. Endrerud, M. Hofmann, R. Martin, and I. B. Sperstad, "Reference Cases for Verification of Operation and Maintenance Simulation Models for Offshore Wind Farms," *Wind Engineering* 39, no. 1 (2015): 1–14.

35. J. Carroll, A. McDonald, and D. McMillan, "Failure Rate, Repair Time and Unscheduled O&M Cost Analysis of Offshore Wind Turbines," *Wind Energy* 19, no. 6 (2016): 1107–1119.

36. ReliaWind, "Reliability Focused Research on Optimizing Wind Energy Systems Design, Operation and Maintenance: Tools, Proof of Concepts, Guidelines & Methodologies for a New Generation," (2011), https://cordis.europa.eu/project/id/212966/reporting.

37. J. McMorland, M. Collu, D. McMillan, and J. Carroll, "Operation and Maintenance for Floating Wind Turbines: A Review," *Renewable and Sustainable Energy Reviews* 163 (2022): 112499.

38. C. Allen, A. Viscelli, H. Dagher, et al., "Definition of the UMaine VolturnUS-S Reference Platform Developed for the IEA-Wind 15-Megawatt Offshore Reference Wind Turbine," NREL, Golden, CO (US, 2020).

39. N. J. Abbas, D. S. Zalkind, L. Pao, and A. Wright, "A Reference Open-Source Controller for Fixed and Floating Offshore Wind Turbines," *Wind Energy Science* 7, no. 1 (2022): 53–73.

40. "IEC 61400-3-1:2019 - Wind Energy Generation Systems–Part 3-1: Design Requirements for Fixed Offshore Wind Turbines," Tech. Rep. (British Standards Institution, London, UK, 2019).

41. G. J. Hayman, "Mlife Theory Manual for Version 1.00," Tech. Rep. NREL, Golden, CO (US, 2012).

42. LAUTEC ESOX, "ERA5 Data Point Map," https://esox.lautec.com/map/.

43. C. Dao, B. Kazemtabrizi, and C. Crabtree, "Wind Turbine Reliability Data Review and Impacts on Levelised Cost of Energy," *Wind Energy* 22, no. 12 (2019): 1848–1871.

44. N. D. Kelley and B. J. Jonkman, "Overview of the TurbSim Stochastic Inflow Turbulence Simulator," Tech. Rep. NREL/TP-500-36971. NREL, Golden, CO (US, 2005).

45. J. McMorland, M. Collu, D. McMillan, and A. Corradu, "The Impact of Limiting Sea States on Floating Offshore Wind Operation and Maintenance," *Applied Oceans Research [under review]* (2023).

46. G. J. W. Van Bussel and W. A. A. M. Bierbooms, "The DOWEC Offshore Reference Windfarm: Analysis of Transportation for Operation and Maintenance," *Wind Engineering* 27, no. 5 (2003): 381–391.